Cell Reports, Volume *27*

Supplemental Information

Molecular Profiling and Functional Analysis of Macrophage-Derived Tumor Extracellular Vesicles

Chiara Cianciaruso, Tim Beltraminelli, Florent Duval, Sina Nassiri, Romain Hamelin, André Mozes, Hector Gallart-Ayala, Gerardo Ceada Torres, Bruno Torchia, Carola H. Ries, Julijana Ivanisevic, and Michele De Palma

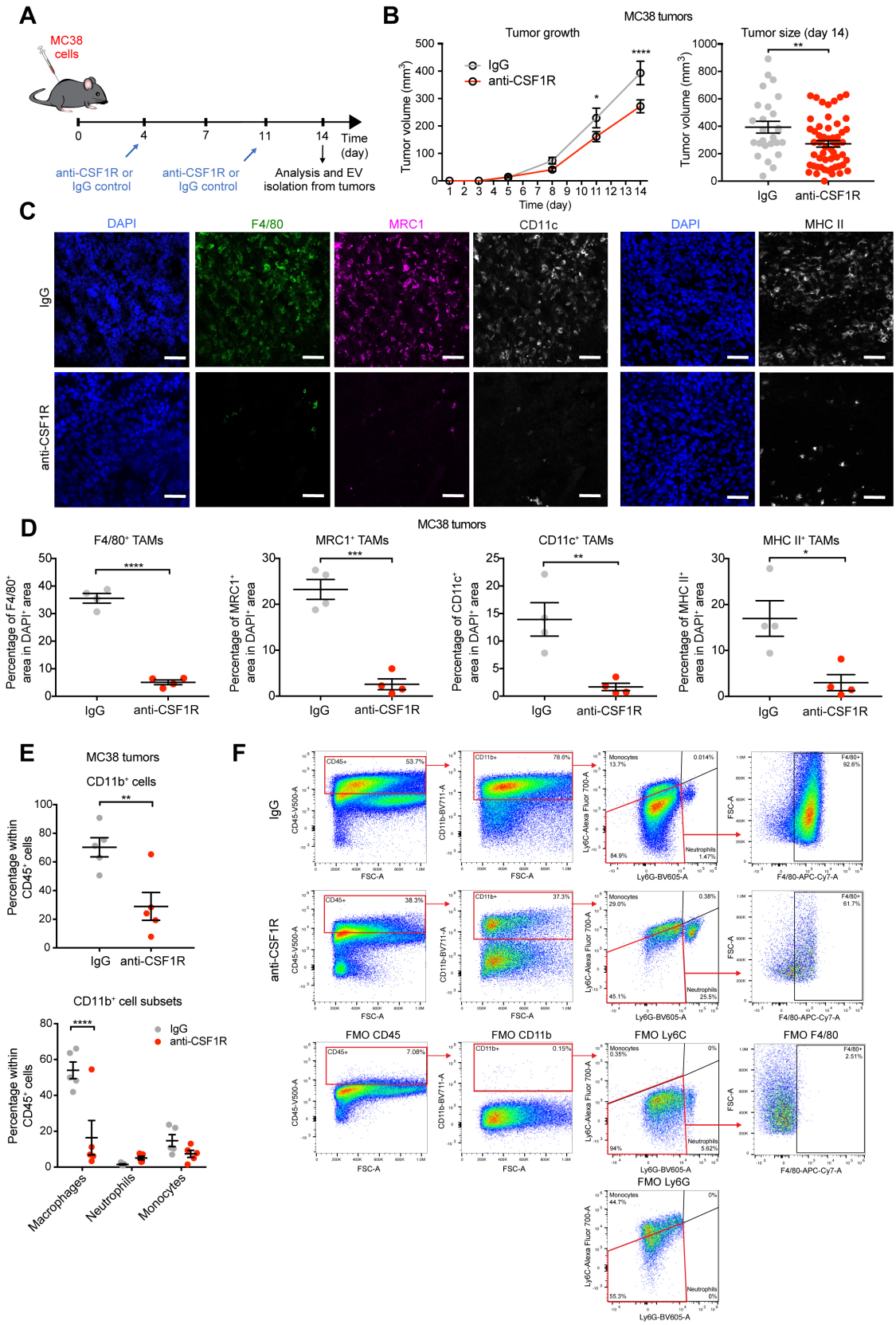

Figure S1. Depletion of macrophages in MC38 tumors by CSF1R blockade, Related to Figure 1

A) Schedule of subcutaneous MC38 cancer cell inoculation and drug administration in C57BL/6 mice.

B) MC38 tumor growth. Left panel shows data as tumor volume (mean ± s.e.m.; n=26-55 mice/condition, from 5 independent experiments combined) at different time-points of analysis. Statistics by two-way ANOVA, using Sidak's multiple comparison test. Right panel shows tumor volume (mean ± s.e.m.) of the same mice at the end

of the experiment (day 14). Statistics by unpaired two-tailed Student's t-test.
C-**D**) Immunostaining analysis of macrophage proteins on MC38 tumor sections. Panels (C) show representative immunostaining images. Nuclei are stained with DAPI (blue). Scale bar, 50 μm. Panels (D) show quantitative analysis of marker-positive area relative to DAPI-positive area (mean ± s.e.m.; n=4 mice/condition; 5 randomly selected images per section). Statistics by unpaired two-tailed Student's t-test.
E) Flow cytometry analysis of myeloid cells in MC38 tumors. Upper panel shows the percentage of $CD11b^+$ myeloid cells within $CD45^+$ hematopoietic cells. Lower panel shows individual myeloid cell types. Data show percentage values (mean ± s.e.m.; n=5 mice/condition). Statistics by unpaired two-tailed Student's t-test (upper panel) and two-way ANOVA, using Sidak's multiple comparison test (lower panel).
F) Representative flow cytometry plots of MC38 tumors showing the gating strategy employed to identify the myeloid-cell populations in (E). FMO, fluorescence minus one (unstained).

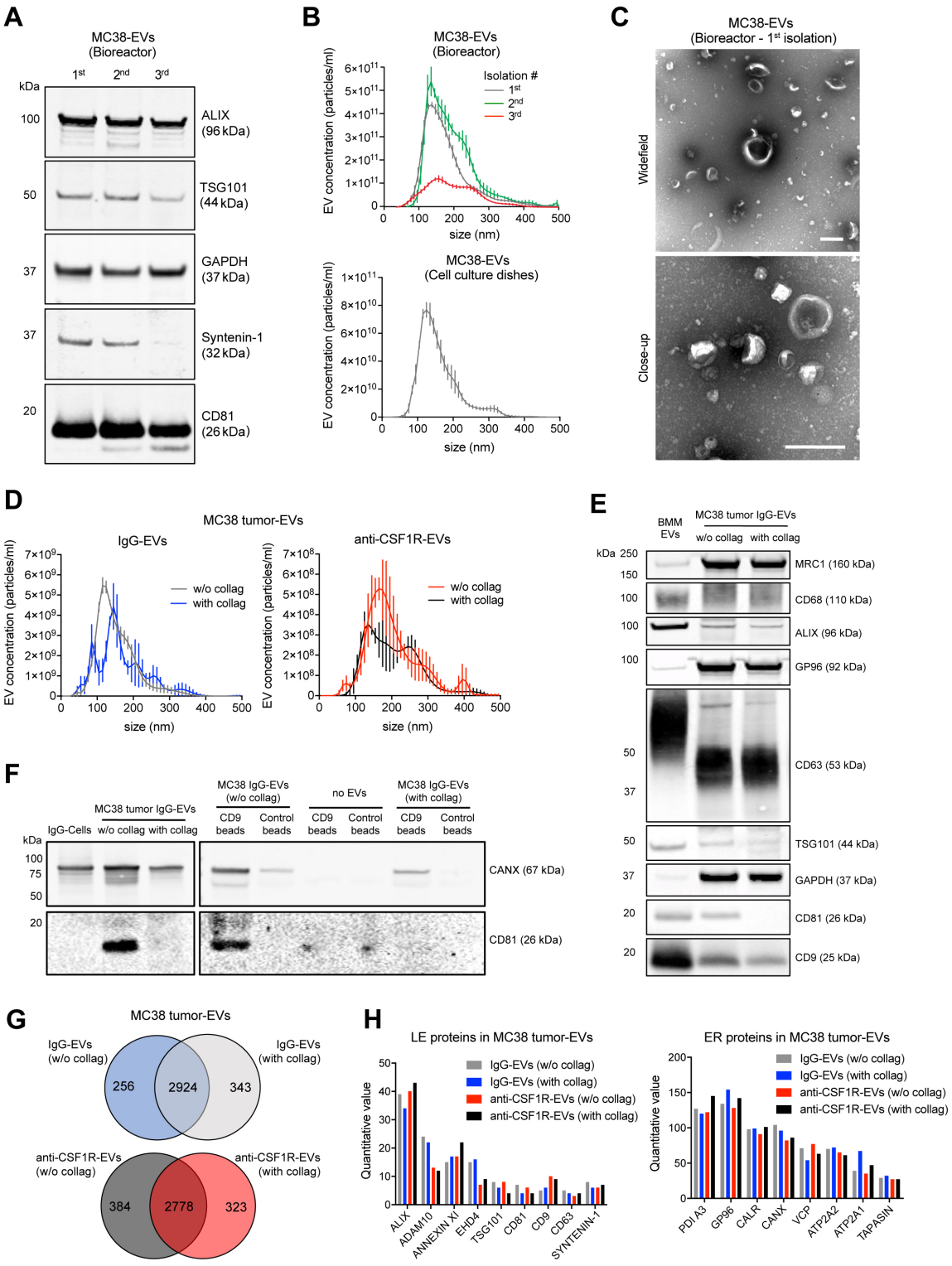

Figure S2. Isolation of EVs from cultured MC38 cells or MC38 tumors, Related to Figure 1

A) WB analysis of three consecutive EV isolations (7 days apart) from MC38 cells cultured in a bioreactor flask.

B) Concentration and size distribution by NTA (mean ± s.e.m.; n=3 acquisitions/sample) of EVs isolated from MC38 cells that were cultured in a bioreactor flask (upper panel) or in standard tissue culture dishes (lower panel). One representative EV preparation per condition is shown.

C) TEM images of EVs from MC38 cells cultured in a bioreactor flask. One representative EV preparation per condition is shown. Scale bar, 200 nm.

D) Concentration and size distribution by NTA (mean ± s.e.m.; n=3 acquisitions/sample) of MC38 tumor-derived IgG-EVs and anti-CSF1R-EVs, extracted with or without (w/o) collagenase. One representative EV

preparation per condition is shown.
E) WB analysis of M2 BMM-EVs and tumor-derived IgG-EVs. One representative EV preparation per condition is shown.
F) WB analysis of tumor-derived cells (IgG-Cells) and IgG-EVs immunoprecipitated with anti-CD9 or control-coated magnetic beads. One representative EV preparation per condition is shown.
G) Venn diagrams comparing proteins detected by LC-MS/MS analysis in IgG-EVs (upper panel) and anti-CSF1R-EVs (lower panel).
H) LC-MS/MS analysis of IgG-EVs and anti-CSF1R-EVs showing proteins identified according to their association with late endosomes (LE, left panel) or endoplasmic reticulum (ER, right panel).

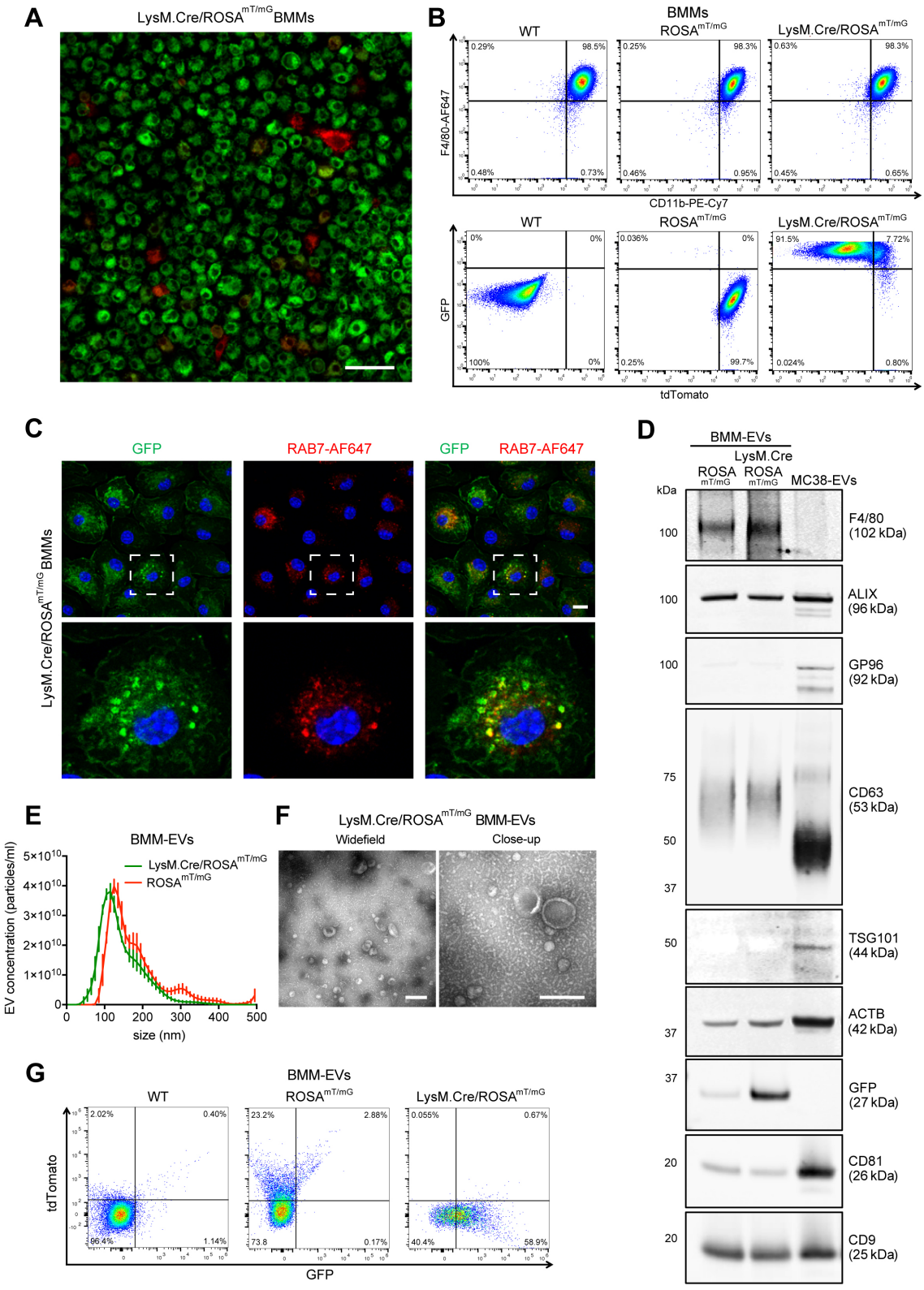

Figure S3. Isolation and characterization of EVs from LysM.Cre/ROSA$^{mT/mG}$ BMMs, Related to Figure 4

A) Live cell confocal imaging of cultured BMMs from LysM.Cre/ROSA$^{mT/mG}$ mice. Scale bar, 50 µm.

B) Flow cytometry analysis of BMMs isolated from wild-type (WT), ROSA$^{mT/mG}$ or LysM.Cre/ROSA$^{mT/mG}$ mice. Representative dot plots show expression of F4/80 and CD11b (upper panels) and GFP and tdTomato (lower panels).

C) Representative confocal images of LysM.Cre/ROSA$^{mT/mG}$ BMMs immunostained for the late endosome antigen RAB7 (red). GFP was detected by direct fluorescence (green). Nuclei are stained with DAPI (blue).

Scale bar, 10 μm.
D) WB analysis of MC38-EVs and EVs from ROSA$^{mT/mG}$ and LysM.Cre/ROSA$^{mT/mG}$ BMMs. One representative EV preparation per condition is shown.
E) Concentration and size distribution by NTA (mean ± s.e.m.; n=3 acquisitions/sample) of EVs isolated from LysM.Cre/ROSA$^{mT/mG}$ and ROSA$^{mT/mG}$ BMMs. One representative EV preparation per condition is shown.
F) Representative TEM images of EVs from LysM.Cre/ROSA$^{mT/mG}$ BMMs. One representative EV preparation per condition is shown. Scale bar, 200 nm.
G) Flow cytometry analysis of EVs isolated from BMMs of WT, ROSA$^{mT/mG}$ and LysM.Cre/ROSA$^{mT/mG}$ mice. Representative dot plots show fluorescence of GFP and tdTomato.

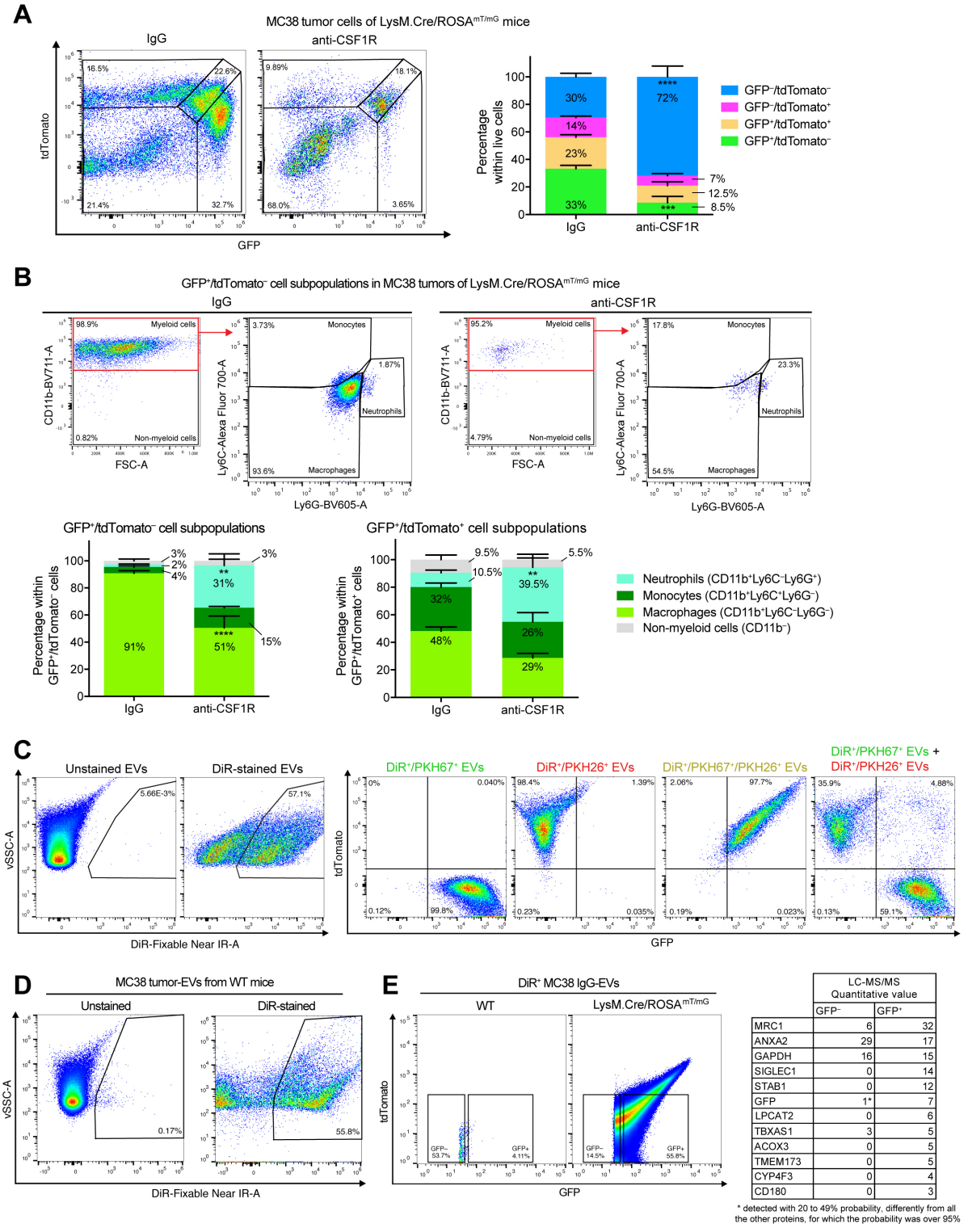

Figure S4. MC38 tumor-derived cell populations in LysM.Cre/ROSA$^{mT/mG}$ mice and sorting of GFP$^+$ EVs, Related to Figure 4

A) Flow cytometry analysis of MC38 tumor-derived cells of LysM.Cre/ROSA$^{mT/mG}$ mice treated with IgG or anti-CSF1R. Left panels show representative flow cytometry dot plots. Right panel shows quantitative percentage values (mean ± s.e.m.; n=5 and 7 mice for IgG and anti-CSF1R, respectively). Statistics by two-way ANOVA, using Sidak's multiple comparison test.

B) Flow cytometry analysis of MC38 tumor-derived GFP$^+$ cells of LysM.Cre/ROSA$^{mT/mG}$ mice treated with IgG or anti-CSF1R. Top panels show representative flow cytometry dot plots. Bottom panels show quantitative percentage values (mean ± s.e.m.; n=5 and 7 mice for IgG and anti-CSF1R, respectively). Statistics as in (A).

C) Flow cytometry analysis of IgG-EVs from MC38 tumors of WT mice. Representative plots show EVs

labeled with different combinations of three fluorescent membrane dyes (DiR, PKH67 and PKH26).
D) Gating strategy employed to identify DiR-labeled EVs in Figure 4C.
E) FACS sorting (dot plots on the left) and LC-MS/MS analysis (table on the right) of GFP^+ and GFP^- EVs ($1x10^6$ each) from IgG-EVs of LysM.Cre/$ROSA^{mT/mG}$ mice.

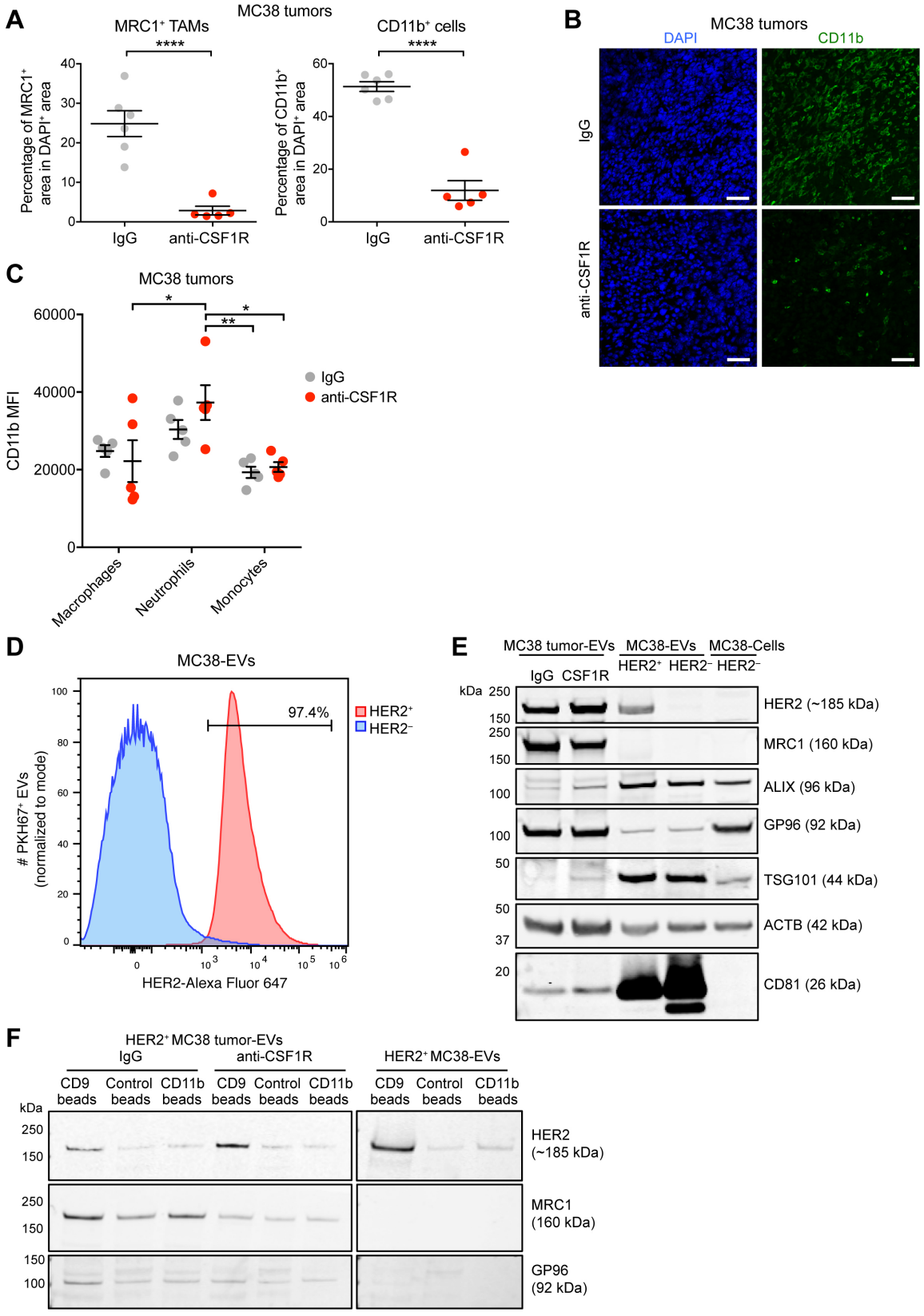

Figure S5. Immunoprecipitation of CD11b⁺ EVs from HER2⁺ MC38 tumors, Related to Figure 4

A) Immunostaining analysis on MC38 tumor sections from IgG- and anti-CSF1R-treated mice, shown as percentage of MRC1⁺ or CD11b⁺ area relative to DAPI⁺ area (mean ± s.e.m.; n=5-6 mice/condition; 5 randomly selected images per section). Statistics by unpaired two-tailed Student's t-test.

B) Representative images showing CD11b immunostaining of tumor sections from the experiment in (A).

Nuclei are stained with DAPI (blue). Scale bar, 50 μm.
C) Flow cytometry analysis showing the median fluorescence intensity (MFI) of CD11b in the indicated myeloid cell types of MC38 tumors of IgG- or anti-CSF1R-treated mice (mean ± s.e.m.; n=5 mice/condition). Statistics by two-way ANOVA, using Tukey's multiple comparison test.
D) Flow cytometry analysis of PKH67-labelled $HER2^+$ and $HER2^-$ MC38-EVs stained with an anti-HER2 antibody.
E) WB analysis of cultured MC38 cells, MC38-EVs, and $HER2^+$ MC38 tumor-derived IgG-EVs and anti-CSF1R-EVs. One EV preparation from a pool of 4 and 6 mice is shown for IgG and anti-CSF1R, respectively. $HER2^+$ MC38 tumors were grown in Wap-*ERBB2* mice. The experiment was performed once.
F) WB analysis of $HER2^+$ MC38-EVs and $HER2^+$ MC38 tumor-derived IgG-EVs and anti-CSF1R-EVs after immunoprecipitation with anti-CD9, anti-CD11b or control-coated magnetic beads. The experiment was performed once.

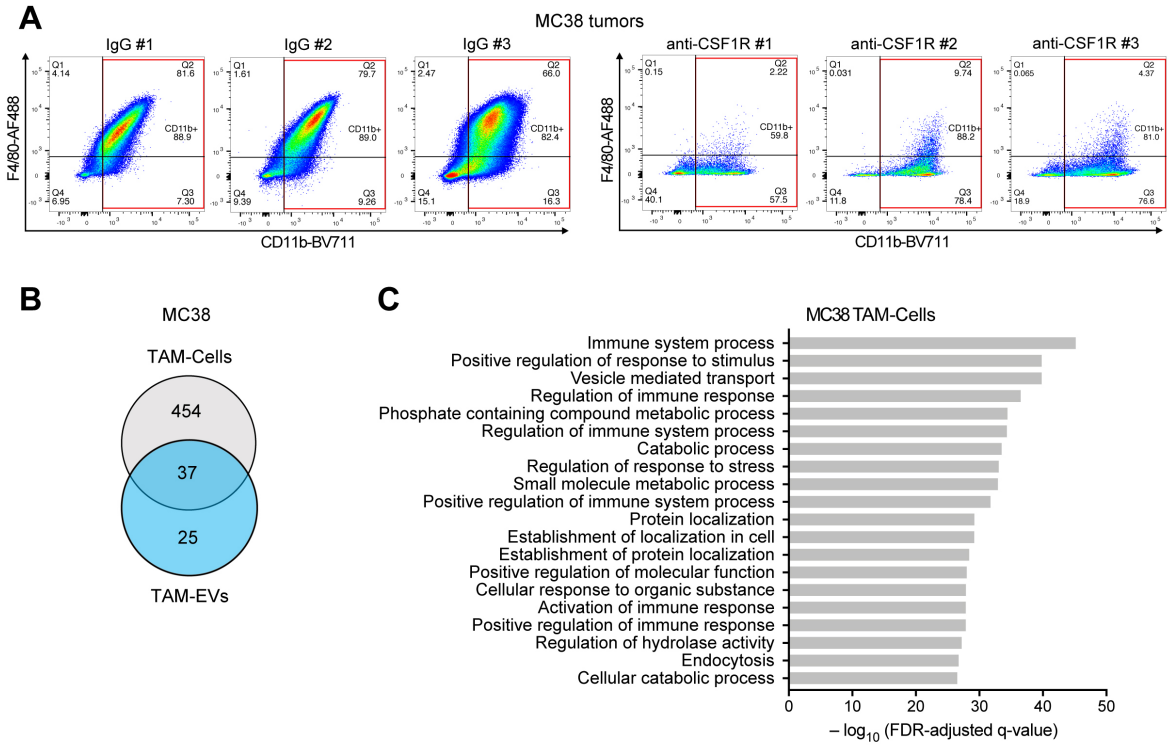

Figure S6. Comparison between TAM-EV and TAM-Cell signatures, Related to Figure 4

A) Flow cytometry of CD11b$^+$ cells in MC38 tumors of mice treated with IgG (left panels) or anti-CSF1R (right panels).

B) Venn diagram comparing proteins of the TAM-Cell and TAM-EV signatures. The TAM-Cell protein signature was determined by LC-MS/MS analysis of FACS-sorted CD11b$^+$ cells and selection of proteins enriched in IgG-Cell versus anti-CSF1R-Cell (criteria: IgG/anti-CSF1R FC>1.7; n=3 tumors/condition).

C) GO enrichment analysis of the TAM-Cell protein signature.

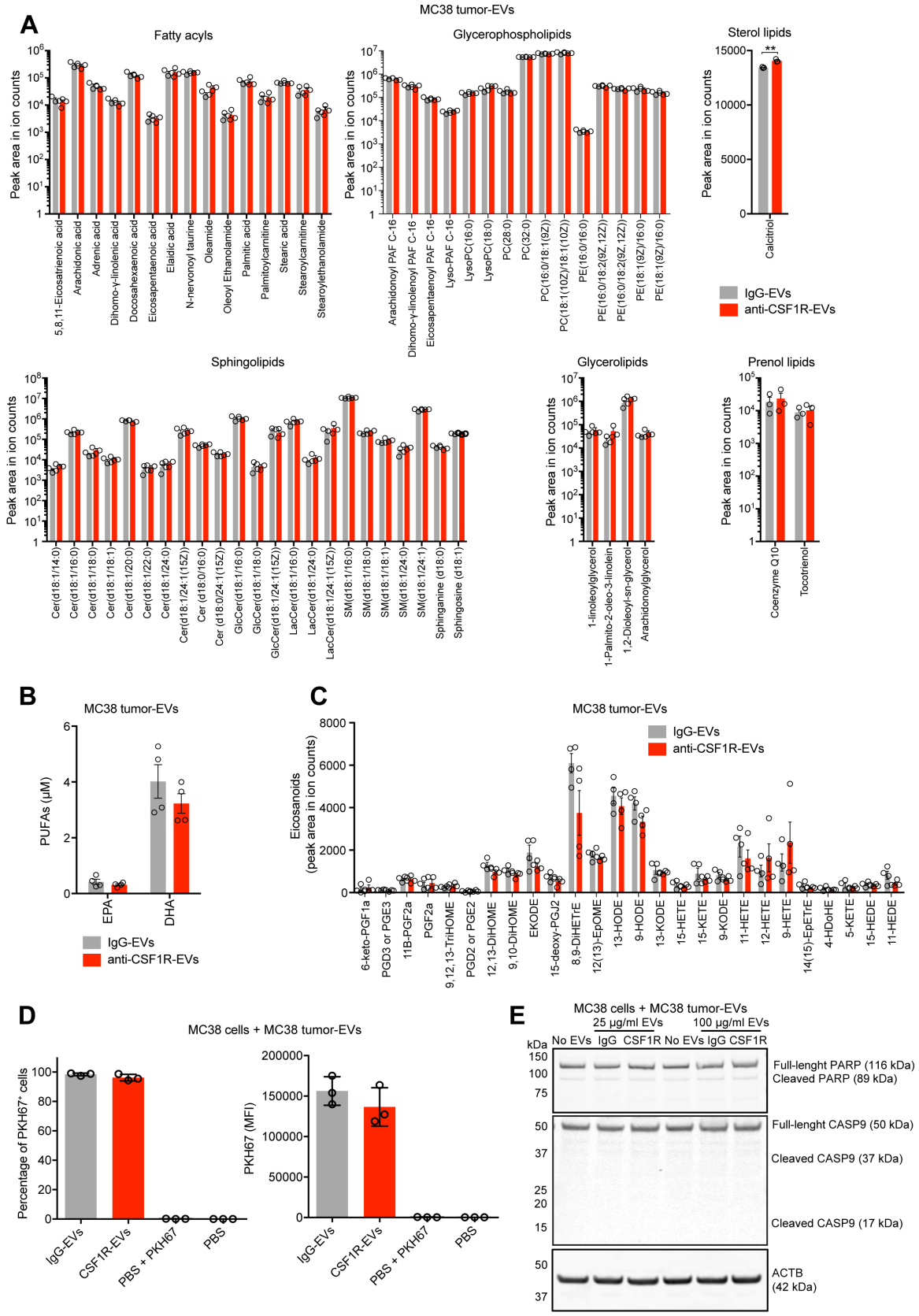

Figure S7. Lipidomic analysis of EVs from MC38 tumors, Related to Figure 6

A) Reversed phase liquid chromatography coupled to high-resolution mass spectrometry (RPLC-HRMS) analysis of some complex lipids detected in IgG-EVs and anti-CSF1R-EVs from MC38 tumors. Data are shown as ion counts (mean peak area ± s.e.m.; n=3 independent EV isolations, each obtained after pooling several tumors). Statistics by unpaired Student's t-test for sterol lipids, and multiple t-tests using Holm-Sidak's multiple

comparison test for all the other lipids.
B) LC-MS/MS-based concentration values of EPA and DHA in IgG-EVs and anti-CSF1R-EVs (mean ± s.e.m.; n=4 independent EV isolations, each obtained after pooling several tumors). Statistics by multiple t-tests using Holm-Sidak's multiple comparison test.
C) LC-MS/MS-based relative quantification of eicosanoids detected in IgG-EVs and anti-CSF1R-EVs (mean ± s.e.m.; n=4 independent EV isolations). Statistics as in (B).
D) Flow cytometry analysis of MC38 cells incubated for 24h with PKH67-labelled IgG-EVs or anti-CSF1R-EVs obtained from MC38 tumors. Data (mean ± s.d.; n=3 independent cell cultures/condition) show percentage values of $PKH67^+$ cells (left panel) or median fluorescence intensity (MFI) of PKH67 (right panel). Statistics by one-way ANOVA, using Tukey's multiple comparison test.
E) WB analysis of MC38 cells incubated for 24h with IgG-EVs or anti-CSF1R-EVs from MC38 tumors. The absence of cleavage and activation of the apoptosis-related proteins PARP and CASP9 indicates lack of activation of apoptotic pathways. The experiment was performed once.